JOURNAL OF MAGNETIC RESONANCE **133,** 266–272 (1998)
ARTICLE NO. MN981461

Intermolecular Zero-Quantum Coherences of Multi-component Spin Systems in Solution NMR

Sangdoo Ahn, Natalia Lisitza, and Warren S. Warren

Department of Chemistry, Princeton University, New Jersey 08544-1009

Received November 17, 1997

Intermolecular zero-quantum coherences (iZQC) induced by the dipolar demagnetizing field can give both *P*- and *N*-type cross peaks. This paper shows that the relative intensities of the two types of iZQC peaks follow a simple relation, $\tan^2(\theta/2)$, from both the quantum (spin density matrix) and classical (modified Bloch equation) calculations. The experimental data and numerical simulations agree well with the prediction. In addition, higher-order iZQCs are experimentally examined for the first time and are explained by the quantum picture in which dipolar couplings convert four-spin operators into observable magnetization.

INTRODUCTION

Numerous 2D NMR experiments in solution give anomalous cross peaks in the indirectly detected dimension because of the dipolar demagnetizing field and radiation damping (*1–13*). Radiation damping is usually the more significant effect with most gradient-free sequences (e.g., a simple COSY-type sequence) (*1, 3, 10*); however, sequences with multiple-quantum selective field gradient pulses (e.g., CRAZED or HOMOGENIZED experiments) to suppress radiation damping exhibit strong cross peaks due to the demagnetizing field (*3, 8, 9, 13*). In uncoupled spin systems (e.g. mixtures of single-line solvents) radiation damping does not generate cross peaks between spins at different resonance frequencies ($|\omega_a - \omega_b| \gg 1/\tau_r$, where τ_r is the radiation damping time) but such inequivalent-spin cross peaks are quite strong with the demagnetizing field (*3*). Hence in the most common case (complex molecules in a concentrated single-line solvent such as water) radiation damping effects are mainly confined to the solvent, but demagnetizing field effects can give solvent–solute cross peaks.

The additional peaks can have >10% of the intensity of the diagonal peaks in a normal COSY experiment and can be quantitatively understood with either classical (modified nonlinear Bloch equation) or quantum (density matrix) treatments. These dipolar demagnetizing field effects, spatially modulated, could act even as a source for extracting structural information (*14, 15*). Hence, understanding the actual physical mechanism for generating a dipolar demagnetizing field may be important. Generally the quantum approach gives a clearer understanding of their physical origin: the peaks come from intermolecular multiple-quantum coherences (iMQCs) which originate in multispin operators in the equilibrium density matrix and are made observable by dipolar couplings.

In recent years, our group has concentrated its attention on intermolecular zero-quantum coherences (iZQCs). Such coherences have magnetic properties that are quite different from the higher MQ coherences (*13, 16*). For example, iZQCs can suppress long-range inhomogeneous broadening since they evolve at the chemical shift differences between two spins. In addition, while MQ-selective experiments using two pulse gradients (dephasing and rephasing) can give only one of the *P*- or *N*-type cross peaks corresponding to the relative direction of two gradient pulses, the HOMOGENIZED sequence $(\pi/2)_y - t_1 - G - \theta_y - t_2$ uses only a dephasing gradient, and hence it can give both the *P*- and *N*-type cross peaks (*13*). The relative intensity of the two types of peaks varies according to the second RF pulse flip angle.

This paper reports analytical solutions for the relative intensities of the two types of peaks in the intermolecular ZQ coherences between two different molecules, from both the quantum (density matrix) and the classical (modified Bloch equation) perspectives. We also present numerical simulations and experimental data for comparison which show various higher-order ZQ coherences (corresponding to four-spin flips) for the first time.

QUANTUM CALCULATION USING DENSITY MATRIX THEORY

The observable zero-quantum coherences can be calculated analytically using both the density matrix and the modified Bloch equation. First we will sketch out the quantum calculation, which readily predicts the relative intensities of the different peaks; then we will derive the explicit analytical expression classically. In the quantum picture we start with the equilibrium magnetization ρ_{eq} for two different kinds spins I and S (uncoupled homonuclear spins) without the high-temperature approximation (*3, 8*)

$$\rho_{eq} = 2^{-(N+M)}\left[\prod_i (\mathbf{1} - \Im I_{zi}) \times \prod_k (\mathbf{1} - \Im S_{zk})\right];$$

$$\Im = 2\tanh\left(\frac{\hbar\omega_0}{2kT}\right), \qquad [1]$$

where the indices i and k run up to the number of I and S spins

1090-7807/98 $25.00

in the sample. The first $\pi/2$ pulse rotates the equilibrium z magnetization into transverse magnetization

$$\rho = 2^{-(N+M)}[\prod_i (\mathbf{1} - \Im I_{xi}) \times \prod_k (\mathbf{1} - \Im S_{xk})], \qquad [2]$$

which contains intermolecular zero-quantum coherences such as $I_{+i}I_{-j}$ and $I_{+i}S_{-k}$ in the $\Im^2$ terms. The second-order terms give double- and zero-quantum coherences,

Only the first two terms are one-quantum coherences and thus can be made observable by commutation with the dipolar couplings. This result implies that the observable signal intensity will be proportional to sin 2θ, and we can get the maximum intensity of the zero-quantum coherence when $\theta = \pi/4$. However, no zero-quantum coherence will be produced by a $\pi/2$ pulse. For the inequivalent-spin case, we have to separate the two zero-quantum coherences since their evolution frequencies during t_1 period differ from each other:

$$I_{+i}S_{-k}(\Delta\omega_I - \Delta\omega_S) = I_{xi}S_{xk} + I_{yi}S_{yk} + iI_{xi}S_{yk} - iI_{yi}S_{xk} \xrightarrow{\theta_y\text{pulse}}$$

$$- \begin{pmatrix} I_{xi}S_{zk}\cos\theta\sin\theta + I_{zi}S_{xk}\cos\theta\sin\theta + iI_{zi}S_{yk}\sin\theta - iI_{yi}S_{zk}\sin\theta \\ + \text{unobservable terms} \end{pmatrix}$$

$$\xrightarrow{I-S\text{ dipolar coupling}} -(I_{yi}\cos\theta\sin\theta - S_{yk}\cos\theta\sin\theta + iS_{xk}\sin\theta + iI_{xi}\sin\theta), \qquad [5]$$

$$I_{-i}S_{+k}(\Delta\omega_S - \Delta\omega_I) = I_{xi}S_{xk} + I_{yi}S_{yk} - iI_{xi}S_{yk} + iI_{yi}S_{xk} \xrightarrow{\theta_y\text{pulse}}$$

$$- \begin{pmatrix} I_{xi}S_{zk}\cos\theta\sin\theta + I_{zi}S_{xk}\cos\theta\sin\theta - iI_{zi}S_{yk}\sin\theta + iI_{yi}S_{zk}\sin\theta \\ + \text{unobservable terms} \end{pmatrix}$$

$$\xrightarrow{I-S\text{ dipolar coupling}} -(I_{yi}\cos\theta\sin\theta + S_{yk}\cos\theta\sin\theta + iS_{xk}\sin\theta - iI_{xi}\sin\theta). \qquad [6]$$

$$I_{xi}I_{xj} = \frac{1}{4}[(I_{+i}I_{-j} + I_{-i}I_{+j}) + (I_{+i}I_{+j} + I_{-i}I_{-j})]$$

$$I_{xi}S_{xk} = \frac{1}{4}[(I_{+i}S_{-k} + I_{-i}S_{+k}) + (I_{+i}S_{+k} + I_{-i}S_{-k})]. \qquad [3]$$

During the delay t_1 the term $I_{+i}S_{-k}$ evolves at the difference of resonance offsets ($\Delta\omega_I - \Delta\omega_S$), the term $I_{+i}I_{-j}$ will not evolve at all if the susceptibility is same in all sample regions. During the first gradient pulse the operator $I_{+i}S_{-k}$ evolves at $(\Delta\omega_I + \gamma Gz_i) - (\Delta\omega_S + \gamma Gz_k)$, the operator $I_{+i}I_{-j}$ evolves at $(\gamma Gz_i - \gamma Gz_j)$.

The second θ pulse transfers these iZQCs into two-spin single-quantum terms such as $I_{xi}I_{zj}$ and $I_{xi}S_{zk}$, which can be rendered observable by a number of small intermolecular dipolar couplings (of the forms $D_{ij}I_{zi}I_{zj}$ or $D_{ik}I_{zi}S_{zk}$). These dipolar coupling operators remove the z term, leaving one-spin single-quantum coherences for detection. For the equivalent-spin case $\frac{1}{4}(I_{+i}I_{-j} + I_{-i}I_{+j}) = \frac{1}{2}(I_{xi}I_{xj} + I_{yi}I_{yj})$

$$\xrightarrow{\theta_y\text{pulse}} \frac{1}{2}(I_{xi}I_{zj}\cos\theta\sin\theta + I_{zi}I_{xj}\cos\theta\sin\theta + I_{zi}I_{zj}\sin^2\theta + I_{xi}I_{xj}\cos^2\theta + I_{yi}I_{yj}). \qquad [4]$$

We can deduce the relative intensity of two observable zero-quantum coherences (*P*- and *N*-type). When spin *I* is detected, the intensity of that coherence can be calculated by taking the trace of the density matrix $\mathrm{Tr}[\rho_I(t_1, t_2)\gamma\hbar(I_x + iI_y)]$. Thus the relative intensity of two observable zero-quantum coherences (*P*- and *N*-type) can be written as the simple relation

$$\frac{M^{+I}(\Delta\omega_S - \Delta\omega_I, \Delta\omega_I)}{M^{+I}(\Delta\omega_I - \Delta\omega_S, \Delta\omega_I)} = \frac{\sin\theta(1-\cos\theta)}{\sin\theta(1+\cos\theta)} = \frac{\sin^2(\theta/2)}{\cos^2(\theta/2)} = \tan^2(\theta/2). \qquad [7]$$

The *S*-spin magnetization is also obtained by simply switching the index *I* to *S*. The relative intensity calculations for these iZQCs induced by dipolar couplings can be directly tested by comparison with numerical simulations and experimental data since the other dynamics effects on both coherences might be similar to each other.

The relative intensity of the four spin related high order zero-quantum terms (in the $\Im^4$ terms), $I_{+i}I_{+j}S_{-k}S_{-l}$ and $I_{-i}I_{-j}S_{+k}S_{+l}$ at $2(\Delta\omega_I - \Delta\omega_S)$ and $2(\Delta\omega_S - \Delta\omega_I)$, can be obtained in a

similar way. The relative intensity relation for all higher-order terms also follows the same relation, $\tan^2(\theta/2)$. However, these peaks are relatively small since they need additional weak dipolar couplings to render them observable.

CLASSICAL CALCULATION USING THE MODIFIED BLOCH EQUATIONS

We introduce the classical calculation based on nonlinear Bloch equations including only the dipolar demagnetizing field (ignoring radiation damping, relaxation, and diffusion), which gives an easy way to predict the signal intensity. At equilibrium the magnitude of the magnetization is given by

$$M_0 = M_0^I + M_0^S. \qquad [8]$$

After the second θ pulse, as well as free evolution during the t_1 and the gradient pulse, the longitudinal and transverse magnetizations are

$$\begin{aligned}
M_z &= -\sin\theta\{M_0^I\cos(\Delta\omega_I t_1 + \gamma GTz) \\
&\quad + M_0^S\cos(\Delta\omega_S t_1 + \gamma GTz)\} \\
M^{I+} &= M_x^I + iM_y^I = M_0^I\{\cos\theta\cos(\Delta\omega_I t_1 + \gamma GTz) \\
&\quad + i\sin(\Delta\omega_I t_1 + \gamma GTz)\} \\
M^{S+} &= M_x^S + iM_y^S = M_0^S\{\cos\theta\cos(\Delta\omega_S t_1 + \gamma GTz) \\
&\quad + i\sin(\Delta\omega_S t_1 + \gamma GTz)\}. \qquad [9]
\end{aligned}$$

After precession during t_2, we have the following equation if the resonance frequencies of two spins differ by much more than the reciprocal of the dipolar demagnetizing time (*8*),

$$\begin{aligned}
M^{I+} &= M_0^I\{\cos\theta\cos(\Delta\omega_I t_1 + \gamma GTz) \\
&\quad + i\sin(\Delta\omega_I t_1 + \gamma GTz)\} \\
&\quad \times \exp i\{\Delta\omega_I t_2 - \sin\theta[\tau_{dI}^{-1}\cos(\Delta\omega_I t_1 + \gamma GTz) \\
&\quad + \frac{2}{3}\tau_{dS}^{-1}\cos(\Delta\omega_S t_1 + \gamma GTz)]t_2\}, \\
M^{S+} &= M_0^S\{\cos\theta\cos(\Delta\omega_S t_1 + \gamma GTz) \\
&\quad + i\sin(\Delta\omega_S t_1 + \gamma GTz)\} \\
&\quad \times \exp i\{\Delta\omega_S t_2 - \sin\theta[\tau_{dS}^{-1}\cos(\Delta\omega_S t_1 + \gamma GTz) \\
&\quad + \frac{2}{3}\tau_{dI}^{-1}\cos(\Delta\omega_I t_1 + \gamma GTz)]t_2\}, \qquad [10]
\end{aligned}$$

where $\tau_{dI} = (\gamma\mu_0 M_0^I)^{-1}$ is the dipolar demagnetizing time of spin *I*. Using the identity

$$\exp(iz\cos x) = \sum_{m=-\infty}^{\infty} i^m J_m(z)\exp(imx), \qquad [11]$$

the observable magnetization becomes

$$\begin{aligned}
M^{I+} = M_0^I &\left[\begin{array}{l} \frac{1}{2}\cos\theta\{\exp i(\Delta\omega_I t_1 + \gamma GTz) + \exp(-i(\Delta\omega_I t_1 + \gamma GTz))\} \\ \quad + \frac{1}{2}\{\exp i(\Delta\omega_I t_1 + \gamma GTz) - \exp(-i(\Delta\omega_I t_1 + \gamma GTz))\} \end{array}\right]\exp i(\Delta\omega_I t_2) \\
&\times \sum_{m=-\infty}^{\infty} i^m J_m\left(-\sin\theta\frac{t_2}{\tau_{dI}}\right)\exp i(m\Delta\omega_I t_1 + \gamma mGTz) \times \sum_{l=-\infty}^{\infty} i^l J_l\left(-\sin\theta\frac{2}{3}\frac{t_2}{\tau_{dS}}\right)\exp i(l\Delta\omega_S t_1 + \gamma lGTz). \qquad [12]
\end{aligned}$$

The *S*-spin magnetization is obtained by simply switching the index *I* to *S*. To find the effect of the spatial modulation imposed by the gradient, we collect all the position-dependent terms as follows:

$$\begin{aligned}
&\{\exp(i\gamma GTz) \pm \exp(-i\gamma GTz)\}\sum_m \exp(i\gamma mGTz) \\
&\quad \times \sum_l \exp(i\gamma lGTz) = \sum_m\sum_l[\exp i\{(1 + m + l)\gamma GTz\} \\
&\quad \pm \exp i\{(-1 + m + l)\gamma GTz\}]. \qquad [13]
\end{aligned}$$

In order for the magnetization to be nonzero after spatial averaging, one of the terms in the sum in Eq. [13] must be constant with respect to position and thus must have a coefficient of zero for *z* direction. Therefore, we require the following condition for there to be a signal: $m + l = \pm 1$. Using the Bessel function relation $J_{-n}(x) = (-1)^n J_n(x)$, we can see that when *l* or $m = 0$, we have cross peaks at the axial positions, (0, $\Delta\omega_I$ or $\Delta\omega_S$):

$$M^{I+} = i\cos\theta\, M_0^I \exp(i\Delta\omega_I t_2) \times J_1\left(-\sin\theta\frac{t_2}{\tau_{dI}}\right)J_0\left(-\sin\theta\frac{2}{3}\frac{t_2}{\tau_{dS}}\right). \quad [14]$$

For $\theta = \pi/2$ (a zero-quantum CRAZED sequence), the equivalent-spin signal will vanish as mentioned earlier. Using the Taylor series expansion $J_1(x) \approx x/2$ for the Bessel function, this equation can be rewritten as

$$M^{I+} \approx -iM_0^I \frac{\sin 2\theta}{4}\frac{t_2}{\tau_{dI}}\exp(i\Delta\omega_I t_2). \quad [15]$$

Thus the flip angle of the second RF pulse to get the maximum coherence is $\pi/4$ (*13*, *16*), which agrees with Eq. [4].

In the case of cross peaks between inequivalent spins, we get more complicated equations. If $l = -k$ and $m = k \pm 1$ then cross peaks appear at $(k(\Delta\omega_I - \Delta\omega_S), \Delta\omega_I)$. Using the Bessel function identities

$$J_{n-1}(x) + J_{n+1}(x) = \frac{2n}{x}J_n(x),$$

$$J_{n-1}(x) - J_{n+1}(x) = 2J_n'(x),$$

$$J_n'(x) = J_{n-1}(x) - \frac{n}{x}J_n(x),$$

the zero-quantum coherence is

$$M^{I+} = -i(-1)^k M_0^I \exp(i\Delta\omega_I t_2)\exp\{ik(\Delta\omega_I - \Delta\omega_S)t_1\} \times \left\{\cos\theta J_{k-1}\left(-\sin\theta\frac{t_2}{\tau_{dI}}\right) - k\frac{(1-\cos\theta)}{\sin\theta}\frac{\tau_{dI}}{t_2} \times J_k\left(-\sin\theta\frac{t_2}{\tau_{dI}}\right)\right\}J_k\left(-\sin\theta\frac{t_2}{\tau_{dS}}\right). \quad [16]$$

This equation implies that high order zero-quantum coherences such as $F_1 = 2(\Delta\omega_I - \Delta\omega_S)$ can be observed, and that the two zero-quantum magnetizations at $\Delta\omega_I - \Delta\omega_S$ (a kind of *P*-type ZQ coherence) and $\Delta\omega_S - \Delta\omega_I$ (a kind of *N*-type ZQ coherence) have different intensities according to the flip angle of the second RF pulse. The magnetization for the cross peak at $(\Delta\omega_I - \Delta\omega_S, \Delta\omega_I)$ is

$$M^{I+} = iM_0^I \exp(i\Delta\omega_I t_2)\exp(i(\Delta\omega_I - \Delta\omega_S)t_1) \times \left\{\cos\theta J_0\left(-\sin\theta\frac{t_2}{\tau_{dI}}\right) - \frac{(1-\cos\theta)}{\sin\theta}\frac{\tau_{dI}}{t_2} \times J_1\left(-\sin\theta\frac{t_2}{\tau_{dI}}\right)\right\}J_1\left(-\sin\theta\frac{2}{3}\frac{t_2}{\tau_{dS}}\right), \quad [17]$$

but that at $(\Delta\omega_S - \Delta\omega_I, \Delta\omega_I)$ is

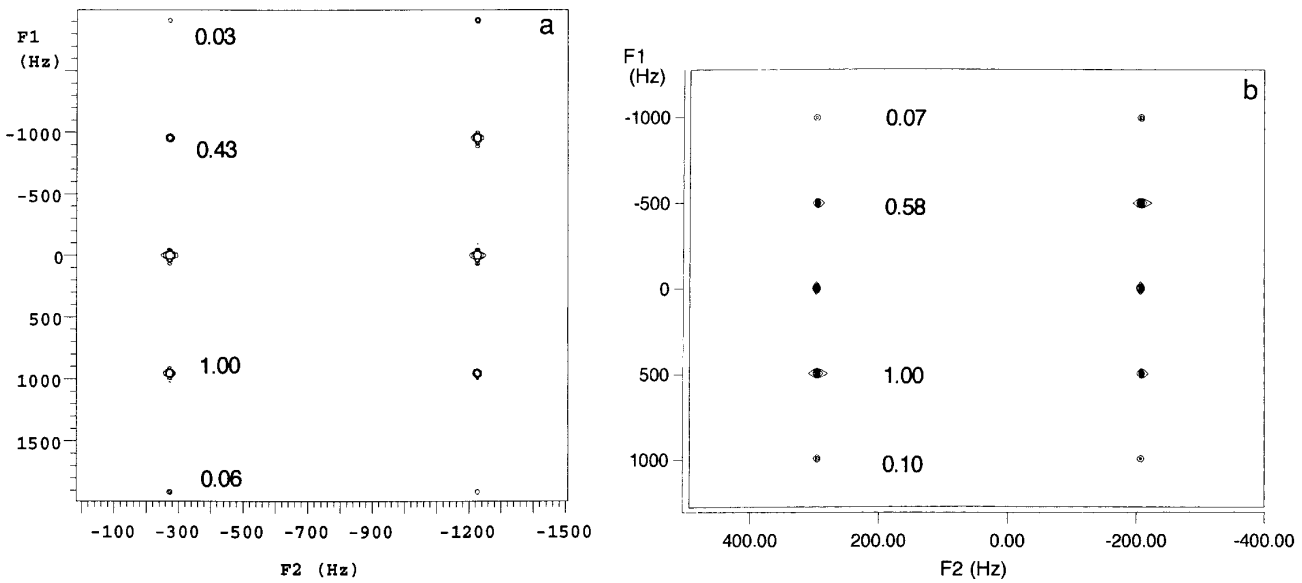

FIG. 1. (a) A two-dimensional spectrum (256 × 1024 data points, $\theta = 75°$) of the intermolecular zero-quantum coherences for a mixture of 50% H_2O and 50% DMSO in the normal tube on a Varian 500-MHz Inova NMR spectrometer at 298 K and (b) corresponding numerical simulation based on the modified Bloch equation including all spin dynamics, relaxation, diffusion, radiation damping, and dipolar demagnetizing field. The relative intensities are listed comparing to the *P*-type two-spin iZQC.

$$M^{I+} = -iM_0^I \exp(i\Delta\omega_I t_2)\exp(i(\Delta\omega_S - \Delta\omega_I)t_1) \times \left\{\cos\theta J_2\left(-\sin\theta\frac{t_2}{\tau_{dI}}\right) - \frac{(1-\cos\theta)}{\sin\theta}\frac{\tau_{dI}}{t_2} \times J_1\left(-\sin\theta\frac{t_2}{\tau_{dI}}\right)\right\} J_1\left(-\sin\theta\frac{2}{3}\frac{t_2}{\tau_{dS}}\right). \quad [18]$$

If we select the relative intensity part from Eqs. [17] and [18], and again use the Taylor series expansions for the Bessel functions, this gives

$$\frac{M^{I+}(\Delta\omega_S - \Delta\omega_I, \Delta\omega_I)}{M^{I+}(\Delta\omega_I - \Delta\omega_S, \Delta\omega_I)} \approx \frac{1-\cos(\theta)}{1+\cos(\theta)} = \frac{\sin^2(\theta/2)}{\cos^2(\theta/2)} = \tan^2(\theta/2), \quad [19]$$

which is exactly the same as the result from the density matrix calculation, Eq. [7]. From Eq. [16], we can also get the intensity information about the high-order zero-quantum coherences at $(2(\Delta\omega_I - \Delta\omega_S), \Delta\omega_I)$ and $(2(\Delta\omega_S - \Delta\omega_I), \Delta\omega_I)$. Using the Taylor series expansions for the Bessel functions, $J_2(x) \approx x^2/8$, the relative intensity is also proportional to $\tan^2(\theta/2)$.

The utility of analytical expressions such as these derives from their predictive power. Changing the second pulse flip angle changes the ratio of the peaks. For $\theta = \pi/4$ the intensity ratio is about 6:1 from Eq. [18]. For $\theta = \pi/2$ the signal does not vanish (unlike the one-component case mentioned earlier), but the ratio is 1:1.

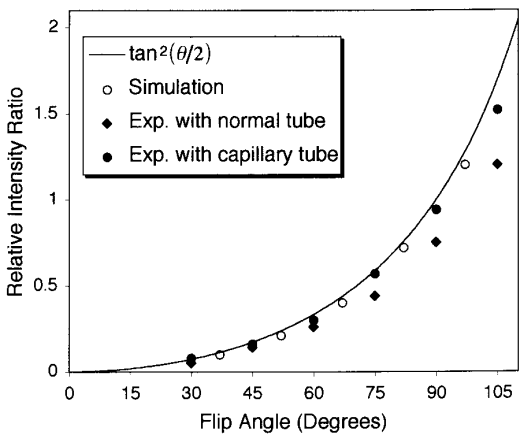

FIG. 2. Comparison of the relative intensities of the *P*- and *N*-types cross peaks in the experimental data. The experimental data from the normal tube show some deviation from the expected curve, while those from the capillary tube show better agreement. A few of the points derived from numerical simulations are also presented for clarity.

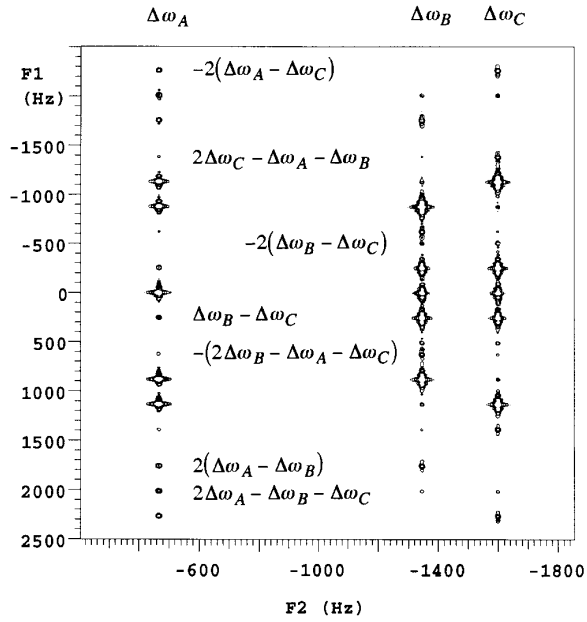

FIG. 3. A two-dimensional spectrum (512 × 2048 data points, $\theta = 90°$) of the intermolecular zero-quantum coherences for a mixture of H_2O, DMSO, and acetone on a Varian 500-MHz Inova NMR spectrometer at 298 K which shows various high-order iZQCs along the indirectly detected dimension. Several representative resonance frequencies along the F_1 axis are marked (see text), where *A*, *B*, and *C* represent H_2O, DMSO, and acetone, respectively. The initial 512 data points in t_2 are truncated to reduce the strong residual magnetization signal while enhancing the signals from the high order iZQCs.

RESULTS AND DISCUSSION

The samples used in the relative intensity study consisted of H_2O and DMSO, placed in a 5-mm NMR sample tube and/or in a 1-mm capillary tube. We added the same amount of acetone for the three-component experiment. All 2D experiments were performed at 298 K using a Varian Unity Inova 500-MHz spectrometer. A gradient of $G = 10$ Gauss/cm was applied along the *z*-direction. The RF pulse width for a flip angle $\pi/2$ is 5.2 μs. The T_1 relaxation times are 1.3 and 2.3 s for H_2O and DMSO, respectively. We set the pulse repetition time enough long to avoid the possibility of stimulated echoes (at least 10 T_1 in every experiment) (*17*, *18*).

Figure 1 shows a zero-quantum 2D-spectrum and a simulation (including all spin dynamics, relaxation, diffusion, radiation damping, and dipolar demagnetizing field) with 75° as the second RF pulse angle. From these results, we can see clearly the high-order zero-quantum coherences at $2(\Delta\omega_I - \Delta\omega_S)$ and $2(\Delta\omega_S - \Delta\omega_I)$ along the indirectly detected dimension even though the intensity is much weaker than those of the two-spin-related zero-quantum coherences. The simulational results (relative intensity) including all mechanisms agree very well with the simple relation, $\tan^2(\theta/2)$, deduced by quantum and classical cal-

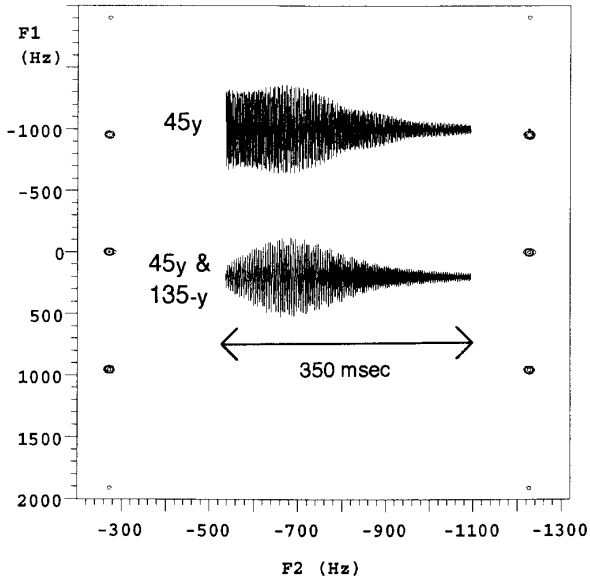

FIG. 4. A two-dimensional spectrum with two FIDs using the pulse sequence to suppress the undesirable axial position signal (changing the second RF pulse from 45_y to 135_{-y} and coadding spectra). The ratio between the intensities of *P*- and *N*-type peaks is nearly 1. The upper FID is obtained from the experiment using 45_y pulse for the second RF pulse while the lower one is obtained from the coadding experiment. Coadding FIDs (mostly iZQC) shows a clearly different profile from those of conventional multiple-spin echoes.

culations in the previous sections which ignored radiation damping, diffusion, and relaxation.

The experimental results also give similar trends, but in the case of the sample in the normal tube, it shows small deviations from the expected results (see Fig. 2). Note there are strong axial position signals (at zero frequency of the F_1 axis) which come from residual *z*-magnetization due to RF pulse imperfections, relaxation and radiation damping during t_1. In addition, strong noise arises all along the F_1 axis since there is no rephasing gradient pulse (selecting only one MQ coherence) after the second RF pulse. Consequently, the total magnetization after the second RF pulse is large enough to generate radiation damping during the t_2 period, and this effect may act as a ''soft'' pulse (*10*). This makes the net effect of the second pulse flip angle smaller, and therefore the relative intensities also should become smaller. However, in the case of the sample in a capillary tube (located inside of a 5-mm normal NMR tube with D_2O), the results agree pretty well with the simple calculational curve because the effects of the radiation damping are negligible in this thin tube. In the case of 80% H_2O and 20% DMSO sample (not shown), each cross peak intensity between inequivalent spins becomes smaller than that in the case of the equivolume sample ($<$50%), and the high-order ZQCs are further reduced ($<$20%). However, the relative intensity still keeps the general rule.

In contrast to the case of two-component system, there are a number of four-spin-related high order zero-quantum coherences in three-component systems such as a mixture of H_2O, DMSO and acetone. In principle, the quantum approach, in this uncoupled inequivalent *ABC*-spin system, can predict and explain that there are 36 kinds of four-spin iZQCs. They can be generated by the combinations of two positive spin operators (I_+^A, I_+^B, I_+^C) and two negative spin operators (I_-^A, I_-^B, I_-^C) at 19 different resonance frequencies (including each axial position) along the indirectly detected dimension. Figure 3 shows all possible four-spin-related iZQCs ($<$10% of two-spin-related iZQCs) in this spin system and can be easily assigned by the quantum approach. For example, the cross peak at ($\Delta\omega_B - \Delta\omega_C$, $\Delta\omega_A$), which cannot be generated by two-spin iZQCs without *J*-coupling, comes from the $I_+^A I_-^A I_+^B I_-^C$ term during the t_1 period. In addition, the intensity of each higher-order iZQC can also be deduced by the quantum approach. For example, the intensity of the iZQC at ($2\Delta\omega_A - \Delta\omega_B - \Delta\omega_C$, $\Delta\omega_A$) corresponding to $I_+^A I_-^B I_+^A I_-^C$ term during the t_1 period is stronger than those of the other spin positions at ($2\Delta\omega_A - \Delta\omega_B - \Delta\omega_C$, $\Delta\omega_B$ or $\Delta\omega_C$). The absence (or weakness) of the cross peaks at ($2(\Delta\omega_A - \Delta\omega_B)$, $\Delta\omega_C$) verifies that the small cross peaks mostly came from four-spin-related iZQCs. We can also see that the simple relative intensity rule works well on this three-component system.

Figure 4 shows a 2D-spectrum and two FIDs using a representative pulse sequence,

$$(\pi/2)_y - t_1 - G - (\theta_y, (\pi - \theta)_{-y}) - t_2,$$

to suppress the undesirable axial position signals. If the second pulse flip angle is changed from $+45°$ to $-135°$ the ZQ coherences (at the axial position) are unaffected, but the coherences from residual *z*-magnetization are inverted. Thus coadding spectra could give mostly ZQ coherences (see FID profiles). Even though this experiment might lose the relative intensity information and could not suppress radiation damping effect in each sequence, the FID signal shows clearly that this coherence differs from just multiple-spin echoes.

CONCLUSION

We produced detailed predictions of the relative signal intensities between *P*- and *N*-type intermolecular ZQ coherences by introducing a simple quantum calculation using the spin density matrix. This is exactly the same as the result of the classical calculation using the modified Bloch equation. We showed that numerical simulations and the experimental data agree very well with this expectation, and that various higher-order iZQCs could be simply explained by the quantum picture.

ACKNOWLEDGMENT

This work was supported by the NIH under Grant GM35253.

REFERENCES

1. M. McCoy and W. S. Warren, *J. Chem. Phys.* **93,** 858 (1990).
2. R. Bowtell, R. M. Bowley, and P. Glover, *J. Magn. Reson.* **88,** 643 (1990).
3. Q. He, W. Richter, S. Vathyam, and W. S. Warren, *J. Chem. Phys.* **98,** 6779 (1993).
4. W. S. Warren, W. Richter, A. H. Andreotti, and S. Farmer, *Science* **262,** 2005 (1993).
5. D. Einzel, G. Eska, Y. Hirayoshi, T. Kopp, and P. Wölfle, *Phys. Rev. Lett.* **53,** 2312 (1984).
6. M. Augustine and K. Zilm, *J. Magn. Reson. A* **123,** 145 (1996).
7. W. S. Warren, S. Lee, W. Richter, and S. Vathyam, *Chem. Phys. Lett.* **247,** 207 (1995).
8. S. Lee, W. Richter, S. Vathyam, and W. S. Warren, *J. Chem. Phys.* **105,** 874 (1996).
9. S. Ahn, W. S. Warren, and S. Lee, *J. Magn. Reson.* **128,** 114 (1997).
10. A. Vlassenbroek, J. Jeener, and P. Broekaert, *J. Chem. Phys.* **103,** 5886 (1995).
11. J. Jeener, A. Vlassenbroek, and P. Broekaert, *J. Chem. Phys.* **103,** 1309 (1995).
12. P. C. M. van Zijl, M. O. Johnson, S. Mori, and R. E. J. Hurd, *J. Magn. Reson. A* **113,** 265 (1995).
13. S. Vathyam, S. Lee, and W. S. Warren, *Science* **272,** 92 (1996).
14. W. Richter, S. Lee, W. S. Warren, and Q. He, *Science* **267,** 654 (1995).
15. R. Bowtell and P. Robyr, *Phys. Rev. Lett.* **76,** 4971 (1996).
16. P. Robyr and R. Bowtell, *J. Magn. Reson. A* **121,** 206 (1996).
17. S. Mori, R. E. Hurd, and P. C. M. van Zijl, *Magn. Reson. Mad.* **37,** 336 (1997).
18. I. Ardelean, R. Kimmich, S. Stapf, and D. E. Demco, *J. Magn. Reson.* **127,** 217 (1997).